

Step-wise change of Asian interior climate preceding the Eocene–Oligocene Transition (EOT)

Hemmo A. Abels^{a,b,*}, Guillaume Dupont-Nivet^{b,c,d}, Guoqiao Xiao^e, Roderic Bosboom^b, Wout Krijgsman^b

^a Stratigraphy/Paleontology, Dept. of Earth Sciences, Utrecht University, Utrecht, The Netherlands

^b Paleomagnetic Laboratory 'Fort Hoofddijk,' Dept. of Earth Sciences, Utrecht University, Budapestlaan 17, 3584 CD, Utrecht, The Netherlands

^c Key Laboratory of Orogenic Belts and Crustal Evolution, Ministry of Education (Peking University), Beijing 100871, China

^d Géosciences Rennes, UMR 6118, Université de Rennes 1, Campus de Beaulieu, 35042 Rennes Cedex, France

^e Key Laboratory of Biogeology and Environmental Geology, Ministry of Education, China University of Geosciences, Wuhan, 430074, China

ARTICLE INFO

Article history:

Received 24 June 2010

Received in revised form 23 November 2010

Accepted 27 November 2010

Available online 9 December 2010

Keywords:

Late Eocene

Doubthouse climate

Eocene–Oligocene Transition (EOT)

Terrestrial record

Gypsum

Red beds

Cyclostratigraphy

ABSTRACT

Understanding the global climate change from greenhouse to icehouse conditions at the Eocene–Oligocene Transition (EOT) 34 million years ago requires climatic records from oceanic as well as continental realms of the key Late Eocene “doubthouse” period preceding this switch. Here, we report integrated stratigraphic results from well-dated Late Eocene continental mudflat to saline lake paleoenvironments of the Xining Basin (northeastern Tibetan Plateau, western China) recording regional and global change. Cyclostratigraphic analysis strongly suggests continuous dominance of the 41-kyr obliquity cycle in the whole late Eocene interval down to the base of polarity chron C18n.2n at 39 Ma with additional input of the ~100-kyr eccentricity cycle up to the base of chron C13r at ~34.7 Ma. This might imply that high-latitude climates dominated the area long before the EOT, probably related to incipient ice-volume fluctuations. Furthermore, our results reveal two paleoenvironmental deterioration steps preceding the Eocene–Oligocene Transition. The first step occurs in the top of chron C17n.1n at ~36.6 Ma. This age closely corresponds to (1) the high-altitude pollen appearance in chron C16.2r at ~36.4 Ma in the same section, (2) the recently dated final retreat of the Tarim Sea in western China, and (3) a shift from precession to obliquity dominance in the Atlantic Ocean. This near co-occurrence suggests global change at this time. We hypothesize this change is related to an increase in incipient ice sheet volume leading to passing threshold conditions for the high-altitude pollen appearance and Tarim Sea retreat, finally leading to decreased moisture availability in the Xining Basin. At the second step, in the base of chron C13r at ~34.7 Ma, a substantial increase in clastic sedimentation rates is observed. This might relate to increased climate variability preceding the greenhouse to icehouse transition at the EOT that prevented landscapes to attain equilibrium configurations.

© 2010 Elsevier B.V. All rights reserved.

1. Introduction

Earth's climate cooled from so-called greenhouse to icehouse climatic conditions from the Early Eocene Climatic Optimum (EECO; ~52–50 Ma) towards the Eocene Oligocene Climate Transition at ~34 Ma (Bijl et al., 2009; Bohaty and Zachos, 2003; Zachos et al., 2001). This deterioration trend is characterised by several, abrupt and transient cooling as well as warming events on time scales of less than 1 million years such as the globally-recognised Middle Eocene Climatic Optimum (MECO) which is accompanied by a preceding cooling event (Bohaty and Zachos, 2003; Bohaty et al., 2009; Coxall et al., 2005). Whereas more and more data is available on the Eocene Oligocene Transition (EOT) interval (Coxall and Pearson, 2007; Zachos et al., 2001), the Late Eocene paleoclimatology is much less well-

resolved. Earth's climate state in this time period has been referred to as the “Late Eocene doubthouse” which refers to the apparent uncertainty if climate will switch back to a full greenhouse state or, as happens at the EOT, finally to a full icehouse state (Pälike et al., 2001). To unravel climate mechanisms in this key period of time, excellent Late Eocene paleoclimate records are available from ocean drilling projects, especially ODP Sites 1218 and 1219. In these sites, Lyle et al. (2005, 2008) observe carbonate accumulation events (CAE's) dated directly and indirectly via magnetostratigraphy. These events are interpreted as precursor events of the deepening of the calcite compensation depth (CCD) at the EOT in reaction to cooling. However, excellently dated terrestrial records over this crucial period of time are needed in order to investigate the potential impact on global climate of CAE's, the MECO, and other steps recognised on the long-term cooling from greenhouse to icehouse conditions in the Late Eocene to Oligocene.

The sedimentary record of the Xining Basin at the north-eastern margin of the Tibetan Plateau in western China is a good candidate to

* Corresponding author. Stratigraphy/Paleontology, Dept. of Earth Sciences, Utrecht University, Utrecht, The Netherlands. Tel.: +31 30 253 5125.

E-mail address: abels@geo.uu.nl (H.A. Abels).

provide such a record due to its thickness and magnetostratigraphic record (Dai et al., 2006; Dupont-Nivet et al., 2007). In this basin, a regional disappearance of gypsum beds intercalated in a dominantly red bed succession has been found to occur exactly at the first step of the EOT and is interpreted as aridification linked to global cooling (Dupont-Nivet et al., 2007; Xiao et al., 2010). Cyclostratigraphic analysis further indicates that the latest Eocene interval in the Xining Basin is characterised by dominant obliquity control on basic mudstone–gypsum cyclicity, interpreted as a high-latitude signal possibly related to incipient ice sheet formation (Xiao et al., 2010). Despite these major findings, the exceptional Xining Basin record still holds critical paleoenvironmental constraints in its downward extension that includes the entire Late Eocene doubt interval. There, spectacular cyclic successions marked by conspicuous stepwise changes in depositional environment need to be described and dated in order to unravel their global vs. regional forcing. Pollen records of the same successions revealed the appearance of high-altitude pollen several million years before the EOT suggesting regional tectonic uplift preceded the EOT (Dupont-Nivet et al., 2008). The retreat of the sea that comprised the Tarim Basin likely occurred during this time interval as well (Bosboom et al., 2011). The retreat of the Paratethys Sea has been suggested to considerably reduce moisture transport to the Xining Basin (Ramstein et al., 1997; Zhang et al., 2007) and, within this reasoning, it seems logic that retreat of the easternmost extend of this sea, the Tarim Sea, might equally lead to aridification in western China.

Here, we present an integrated stratigraphic analysis of the excellently preserved sedimentary record of the Late Eocene found at the Shuiwan section in the Xining Basin including the downward extension and refinement of a previous magnetostratigraphic age model (Dupont-Nivet et al., 2007). Detailed sedimentologic and cyclostratigraphic analyses are performed to examine the paleoenvironmental significance of conspicuous stepwise changes found in the section.

2. Geological background and sampling

The Xining basin is part of a large Paleocene–Miocene basin system characterised by upward fining sediments associated with low accumulation rates in the order of 1–10 cm/kyr. They are attributed to regional post-rift thermal subsidence subsequent to Mesozoic extension (Dupont-Nivet et al., 2004; Horton et al., 2004). The stratigraphic base of the studied interval is found disconformable on the Late Cretaceous Minhe group. This basal relationship extends to the east in the adjacent Lanzhou Basin where thicker conglomeratic series are found unconformable on folded Cretaceous rocks suggesting post Cretaceous tectonism east of the Xining Basin followed by regional subsidence and basin initiation or re-activation (Zhai and Cai, 1984). Magnetostratigraphic dating of the particularly well-developed >1000-m-thick Cenozoic stratigraphy of the Xining basin indicates sub-continuous deposition between ~52 Ma to 17 Ma (Dai et al., 2006). The stratigraphy consists of basal sandy successions (Qiejia-chuan formation, >52 Ma) overlain by red mudstones with distinctive gypsiferous intercalations (Honggou and Mahalagou formations, ~52–30 Ma) overlain by light brown to yellow mudstones with occasional sandy lenses (Xiejia, Chetougou and Xianshuihe formations ~30–17 Ma). Apart from the disappearance of gypsum intercalation that is precisely correlated to the Eocene–Oligocene climate transition (Dupont-Nivet et al., 2007; Xiao et al., 2010), deposition is virtually undisturbed with slow accumulation (average 2.2 cm/kyr) until 17 Ma. This suggests that important deformation did not affect the Xining Basin until that time. A post-17 Ma age is hence indicated for the observed deformation of the strata by a set of regional E–W and local NW–SE structures.

We focus here on the record leading to the EOT that is included in the Mahalagou formation, composed of intercalations of layers of

gypsum within red mudstone successions up to the EOT where the gypsum disappears. Previous lithofacies analyses of the Xiejia and Shuiwan sections (Fig. 1) showed that gypsum/gypsiferous layers were formed during periods of relatively higher water supplies to a (ephemeral) shallow saline lake, while mudstone layers developed in more arid periods in a distal alluvial fan environment (Dupont-Nivet et al., 2007). We provide here detailed lithofacies description leading to in-depth interpretations of depositional environments.

Further paleoenvironmental insights have been provided by pollen recovered from gypsiferous beds of the playa deposits (Dupont-Nivet et al., 2008). The pollen record throughout the Eocene to Oligocene sediments is dominated by xerophytic taxa (*Ephedra* and *Nitraria*) indicating dry desert to steppe environments in agreement with the playa lithofacies. Within the Mahalagou Formation, a change to higher altitude conditions in the surrounding paleoenvironments is indicated by the overwhelming and regional appearance of representatives of the Pinaceae family – and in particular that of *Picea* – which dominate the modern high-altitude palynological record (Lu et al., 2007). This sudden change occurring several million years before the Eocene–Oligocene boundary was thus interpreted as an expression of the long-term regional uplift reported in the central Tibetan Plateau (Wang et al., 2008) possibly associated with short term climate variations explaining the abrupt character of the change. We will provide here a revised age for the high-altitude pollen appearance and place it in light of paleoenvironmental variations revealed by lithofacies and lithostratigraphic changes.

Our sampling thus focused on the stratigraphic interval of the Late Eocene Mahalagou formation including both records of high-altitude pollen appearance and of the aridification that occurs during the EOT. Both events are clearly expressed by sharp changes in lithological characters. These stepwise changes subdivide the studied sedimentary successions into three distinctive intervals with upwards increasing mud/gypsum ratios: (1) the gypsum-rich ‘lower interval’ below the high-altitude pollen appearance, (2) the mudstone-rich ‘upper interval’ above the high-altitude pollen appearance and (3) the exclusively mudstone ‘Oligocene interval’ after the gypsum disappearance above the EOT. To determine the age and understand the paleoenvironmental significance of these lithologic changes, the Shuiwan section was measured and described lithologically at 10 cm resolution (using a Jacob’s staff) through a ~200 m-thick continuous interval (Fig. 1). Samples were collected throughout for magnetostratigraphy, sedimentology, and isotope analysis.

3. Results

3.1. Sedimentology and basic cycling

First, mudstone and gypsum lithologies are described and interpreted separately. This is followed by descriptions and paleoenvironmental interpretations of the characteristic mudstone–gypsum cycles found in the lower interval (below the high-altitude pollen appearance) and in the upper interval (above the high-altitude pollen appearance). Here we discuss the Eocene part of section only, for the Oligocene interval and the Eocene–Oligocene Transition (EOT) we refer to Dupont-Nivet et al. (2007); Xiao et al. (2010).

3.1.1. Mudstones – description

The Shuiwan section is characterised by reddish brown to dark reddish brown (hues of 5YR 4/6–8 and 2.5–5YR 3/4–6, respectively), silty mudstones intercalated by gypsum beds at meter-scale. Mudstones are massive and homogeneous (Fig. 2A) throughout the entire succession and without apparent change between the lower and upper intervals. Occasionally they display variable amounts of dispersed very fine to fine-grained, sometimes lenticular gypsum grains. All mudstones lack sedimentary structures at outcrop scale indicative of depositional mechanism and pedogenesis. Less common are greyish

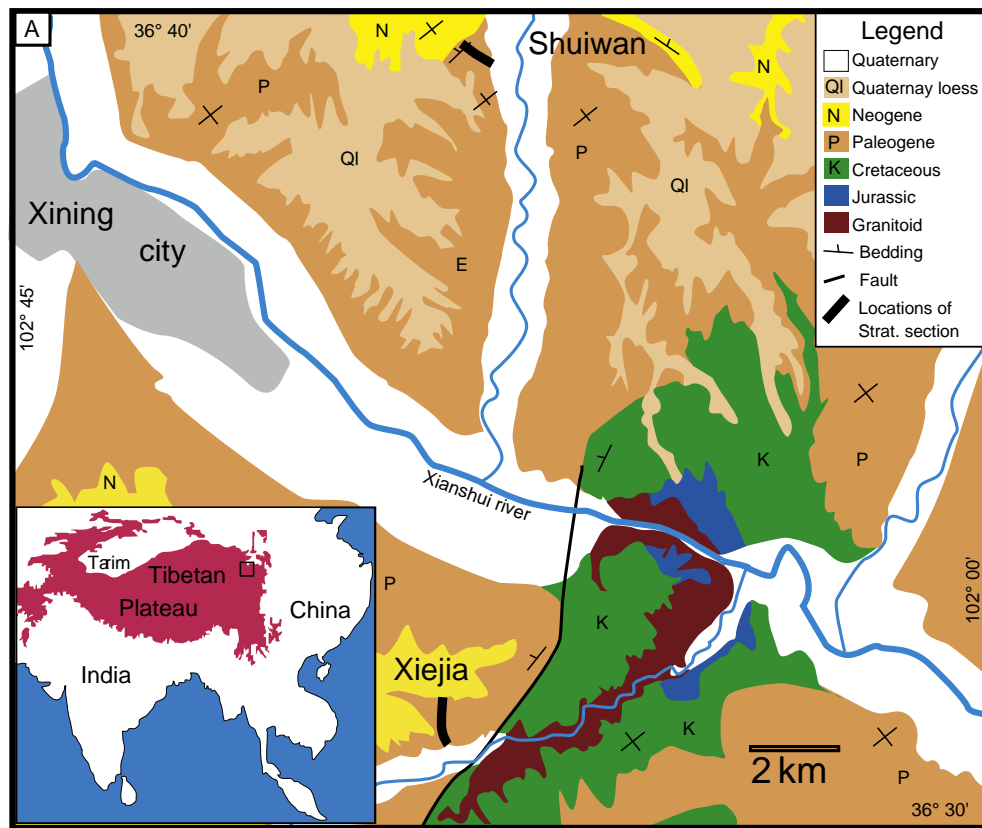


Fig. 1. Geologic setting and location of the Xining basin stratigraphic sections – Strat. section. Redrawn from Dupont-Nivet et al., 2007.

olive, massive and homogeneous, occasionally gypsiferous, mudstones (Fig. 2A and B). These occur mainly below and locally above gypsum beds, and occasionally as separate beds in the reddish-brown mudstones. Contacts between reddish-brown and greyish-olive mudstones are relatively sharp.

3.1.2. Mudstone – interpretation

We interpret the massive reddish-brown mudstones as oxidised, subaerial deposits of a low-gradient floodplain or dry mudflat environment. Absence of original sedimentary structures indicative of transport mechanisms can be due to weak pedogenic alteration, compaction, and drying and wetting of the sediment after deposition. Alternatively, these might be absent due to eolian origin of siliciclastic sediments (Abels et al., 2009; Wright and Marriott, 2007). The absence of colour mottling, carbonate nodules or gley-features might indicate that the paleoenvironment was too dry for significant pedogenesis and soil formation after deposition. The fine-grained interstitial and occasionally lenticular gypsum grains have likely been precipitated from evaporating phreatic groundwater or occasional surface waters percolating into the sediment although a (partial) secondary origin of these gypsum grains can never be excluded. The greyish-olive mudstones are interpreted as sediments deposited in a reducing environment during times of (seasonal) standing water conditions.

3.1.3. Gypsum beds – description

Throughout the section, gypsum beds vary in thickness between 0.1 and 2.5 m. All beds show variable amounts of reddish-brown (hues of 5YR 4/6–8) and greyish-olive (hues of 5–7.5Y 5/2–4) mud. Most gypsum beds, especially in the lower interval of the section, show white and powdery nodular character, which occurs more in natural outcrops than in freshly excavated outcrops (especially quarries). Nodule size

ranges between a few millimetres to commonly a few centimetres. Three predominant gypsum facies were recognised:

- (1) Fine-grained massive gypsum beds that are grey to greyish-olive and occasionally display decimetre-scale bedding (Fig. 2E). Centimetre-size nodular character and bedding in these beds especially occurs at their bases and tops.
- (2) Laminated gypsum beds that display millimetre to centimetre-scale (very) fine-grained gypsum laminae. Greyish-olive laminated beds occur with gypsum laminae densely packed without significant mud present in the gypsum or in between gypsum laminae (Fig. 2D). Also, reddish-brown laminated beds occur that show gypsum laminae separated by thin red mudstone laminae (Fig. 2C). These laminae can undulate and occasionally pinch out thereby mimicking small-scale cross-bedding, which however can hardly be distinguished from disturbance by diagenesis and small-scale tectonic movements along joints.
- (3) Gypsum beds consisting of centimetre- to decimetre-thick layers of lenticular and prismatic gypsum crystals of 1 to 3 cm in size. The crystals are slightly preferentially non-horizontally oriented occasionally in rosette-like aggregates (Fig. 2F). Reddish-brown mud occurs in association with these deposits with different amounts.

3.1.4. Gypsum beds – interpretation

The gypsum facies presented here are related to deposition in saline lake and mudflat environments. The nodular character is interpreted to be partly related to surface ‘alabastrisation’ during weathering in natural outcrops, because alabastrine nodular character is more present in weathered natural outcrops than in fresh outcrops. Part of the nodular alabastrine character might be related to a syndimentary origin due to repeated drying and wetting in the

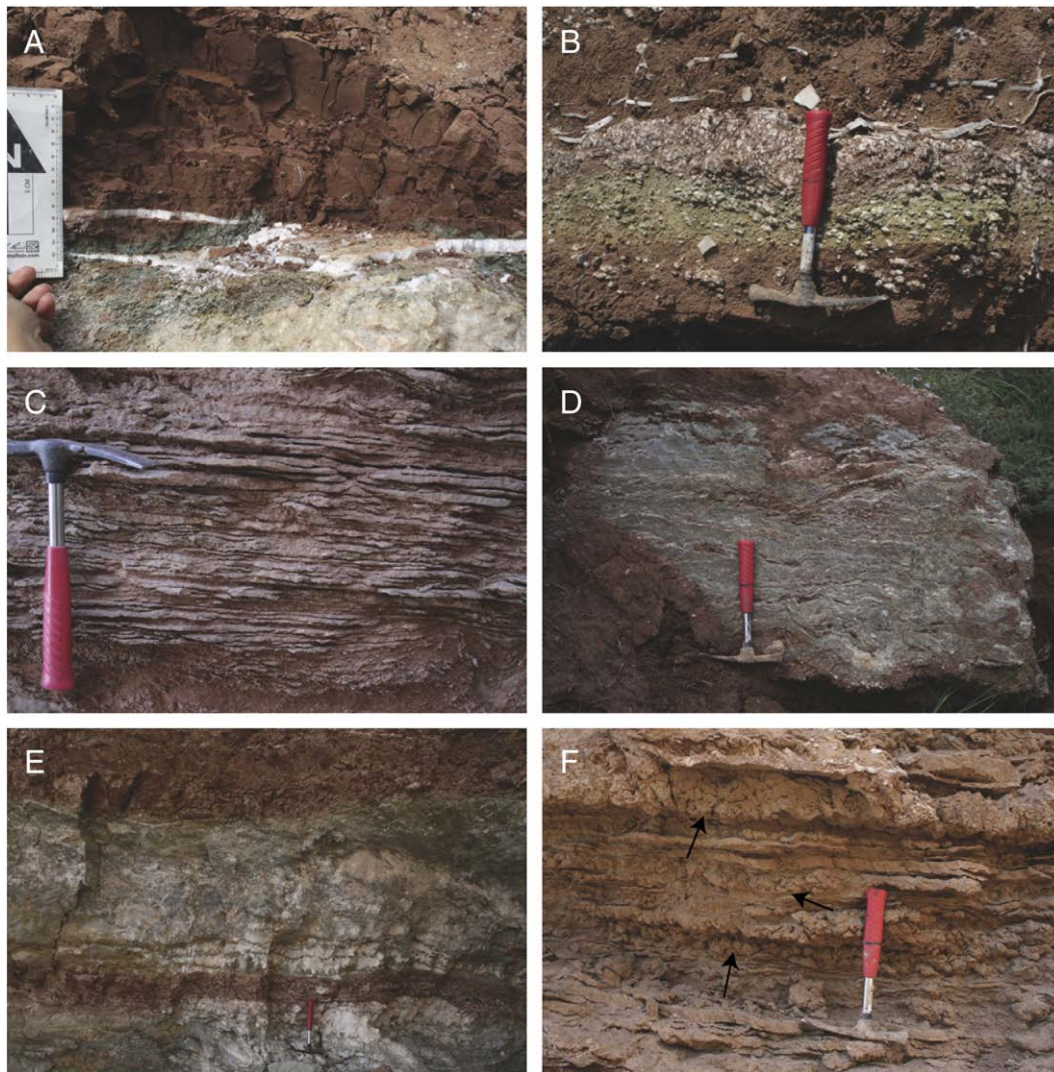


Fig. 2. Photographs from sedimentological features in the Shuiwan section. For scale, red handle of hammer, 18 cm long, and white scale bar, 15.3 cm long with metric subdivision. A) Detail of a transition from olive-grey to reddish-brown mudstone, B) a thin nodular gypsum bed showing the characteristic pattern from red mud to green mud to green muddy gypsum back to red mud, C) red laminated gypsum bed with gypsum laminae separated by mud laminae, D) densely-packed green laminated gypsum bed, E) massive, nodular grey gypsum bed showing bedded structure mainly at its base, and F) beds of euhedral gypsum crystals mimicking rosette-like structures.

marginal zone of the saline lake system during shrinking stages of the playa lake (Ortí et al., 2007; (Warren, 2006; Fig. 2B). The fact that this nodular character is more often observed in the bases and tops of the massive gypsum beds might indicate an early-diagenetic origin.

The interpretations of the predominant gypsum facies are as follows:

- (1) The massive, fine-grained gypsum beds are interpreted as deposits from ephemeral to perennial saline lake environments (Ortí et al., 2007). The near lack of mud in these beds indicate that both eolian and lacustrine siliciclastic input was very low suggesting a relative distal position within the lake system and/or enhanced vegetation cover at the margins hampering surface and eolian transport.
- (2) The densely-packed laminated gypsum beds that occur in association with low amounts of green mud are similarly interpreted as deposits from an ephemeral to perennial saline lake environment (Ortí et al., 2007). On the other hand, the laminated gypsum beds showing mud laminae between gypsum laminae might indicate less stable, probably ephemeral, saline lake environments and/or less vegetation cover

(Ortí et al., 2003). Also, some of the gypsum laminae might be the result of transport and clastic redeposition of gypsum (gypsarenite) which is further suggested by the possible cross-beds in these facies (Ortí et al., 2007).

- (3) The dispersed lenticular gypsum crystals within red mudstones as well as the beds of lenticular and prismatic gypsum crystals are interpreted as interstitial gypsum deposits at the top of the phreatic groundwater level below ground surface of a dry mudflat at the lake margin (Ortí et al., 2007; Warren, 2006). The thicker intervals with centimetre-size lenticular gypsum crystals resemble typical 'desert rose' gypsum formation that indicate prolonged periods of phreatic groundwater levels (seasonally) close to ground surface (Warren, 2006).

3.1.5. Mudstone–gypsum cycles – description

Throughout the Shuiwan section changes occur in the character and the thickness of the basic mudstone–gypsum cycle. Here, we discuss two generalized basic cycles that depict the characteristics of the mudstone–gypsum cycling in the distinctive lower and upper part of the section (below and above the high-altitude pollen appearance).

Arbitrarily, we start these basic cycles with mudstone followed by gypsum.

3.1.5.1. Lower interval – cycles –23 to 20. The generalised basic cycle for the lower part of the section has a thickness of around 1 m and starts with a reddish-brown mud containing abundant dispersed alabastrine gypsum nodules interpreted as saline mudflat deposit with occasional phreatic groundwater levels close to ground level (Fig. 3A). This is followed by a relatively sharp transition to a greenish-olive mudstone interval that shows variable amounts of dispersed gypsum nodules which, slightly higher upsection, occur as green muddy nodule beds. This interval is interpreted as deposited in the marginal zone of a saline lake system. Above, a massive, bedded, locally alabastrine nodular, greyish-olive gypsum occurs that is only occasionally disrupted by thin greenish-olive mud layers. This interval is interpreted as deposited in an ephemeral to perennial saline lake system. The top of this interval is characterised by more mud-rich and more nodular and bedded strata indicating the relatively rapid disappearance of the saline lake system.

3.1.5.2. Upper interval – cycles >20 to 61. The generalised basic cycle for the upper part of the section is generally thicker between 2 and 5 m, although in the first half of this interval around 1-meter-thick cycles occur as well. The typical cycle starts with a much thicker reddish-brown mudstone similarly interpreted as dry mudflat deposits. Mudstones contain interstitial, very-fine-grained lenticular gypsum crystals (Fig. 3B). Towards the gypsum bed on top, thin laminae of gypsum occur and occasionally laminae or beds of lenticular and prismatic gypsum crystals indicating gradual (seasonal) rising of groundwater levels. The basal part of the gypsum bed consists of centimetre-size lenticular and prismatic gypsum crystals indicating prolonged times of phreatic groundwater levels close to ground level without significant times of a stable water body in a saline lake environment. The upper part of the gypsum bed, first consists of fine-grained laminated gypsum, with red mud separating the gypsum laminae, followed upward by a densely-packed laminated green gypsum indicating the transition to ephemeral to perennial saline lake environments. The uppermost part of the gypsum bed shows a rather rapid shift to red mudstone lithology, again indicating rapid disappearance of the saline lake.

3.1.6. Mudstone–gypsum cycles – interpretation

The transition from red bed to gypsum deposition is interpreted to indicate the transition from paleoenvironments that on long time

scales (10^3 – 10^4 years) can be characterised as dominantly dry (subaerially-exposed mudflat or clay pan) towards less dry (saline mudflat and saline lake) environments. Remarkably, the lithofacies cycles reveal relatively sharp shifts from dry mudflat environments to saline lake environments and vice versa in most cycles without much indication of intermediate environments or switching between the two states on short time scales (10^1 – 10^2 years). Apparently, a robust forcing mechanism existed causing repeated switching between the two states on 10^3 to 10^4 years time scales.

In the following, we argue that water availability and therefore local or regional precipitation was the controlling factor for the repeated development of stable water bodies in a saline lake environment in the otherwise dry mudflat environment. Deposition of gypsum requires 1) time, 2) solutes, 3) net positive evaporation/water influx ratio, and 4) the availability of water (Rosen, 1994; Yechieli and Wood, 2002). Previous age control already indicated that sedimentation rates are low (2–5 cm/kyr) in the Shuiwan section and the central Xining Basin in general (Dai et al., 2006; Dupont-Nivet et al., 2007), suggesting time was not a limiting factor. The presence of gypsum beds throughout the Shuiwan section as well as in the stratigraphic interval below the section (Dai et al., 2006) suggests that gypsum–solute were constantly present in the area and argue that on time scales of the basic cyclicity availability of gypsum solute sources was not a limiting factor either. Both mudstone and gypsum lithofacies and pollen data indicate (semi-)arid paleoenvironments with high evaporation rates. Therefore, we argue that the controlling factor is water availability, which is now corroborated by our lithofacies analysis. The red mudstone intervals do not show significant pedogenic alteration, which is remarkable when ample time is available. This suggests red mudstone intervals characterise very low groundwater and phreatic water levels and paleoenvironments too dry for significant paleosol formation. We reject the possibility that the hampered soil formation is due to poor drainage because this would lead to significant interstitial gypsum precipitation at the phreatic groundwater level which is not observed. In contrast, thick gypsum intervals characterise groundwater levels close to or above ground level during sufficient time to transport solutes and precipitate significant gypsum beds with mostly no intercalation of red muds (Rosen, 1994; Yechieli and Wood, 2002). The switch from groundwater levels far below ground level during red mudstone deposition to groundwater levels near ground level during gypsum deposition, suggests not evaporation but precipitation was the limiting factor for gypsum deposition in the Shuiwan section. Yechieli and Wood (2002) emphasize that in most playa systems the amount of surface water influx is much less than the contribution of groundwater to filling a saline lake and so, likely, groundwater influx and thus rainfall on the surrounding regions was the governing factor.

3.2. Lithostratigraphy

The character of the gypsum–mudstone alternations and the type of gypsum beds change considerably through the Shuiwan section. Therefore, the Eocene part of the Shuiwan section has been subdivided into two intervals as was done in Section 3.1.5 for the basic cycle description. A depth rank series has been constructed at a 10-cm resolution, in order to perform time series analysis for cyclostratigraphic investigation. Ranks are defined from 1 to 7 depending on the supposed water availability in the system, according to the environmental interpretation of lithofacies described above. Ranks vary from 1 for (dark-)reddish brown mudstone, 2 for greyish-olive mudstone, 3 for nodular reddish-brown gypsum, 4 for nodular greyish-olive gypsum, 5 for laminated reddish-brown gypsum, 6 for laminated greyish-olive gypsum, and 7 for massive greyish-green gypsum. Intermediate values were used when laminae of gypsum beds were clearly separated by thin mudstone laminae,

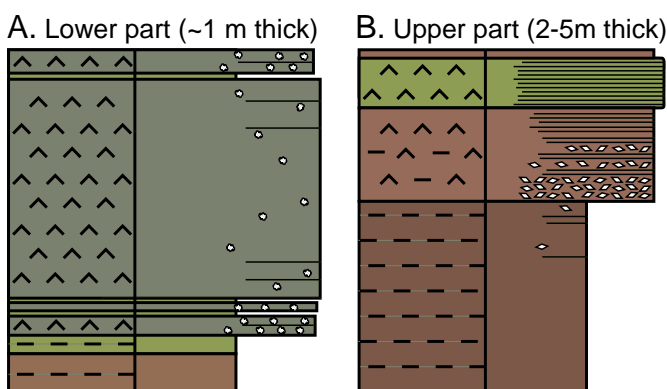
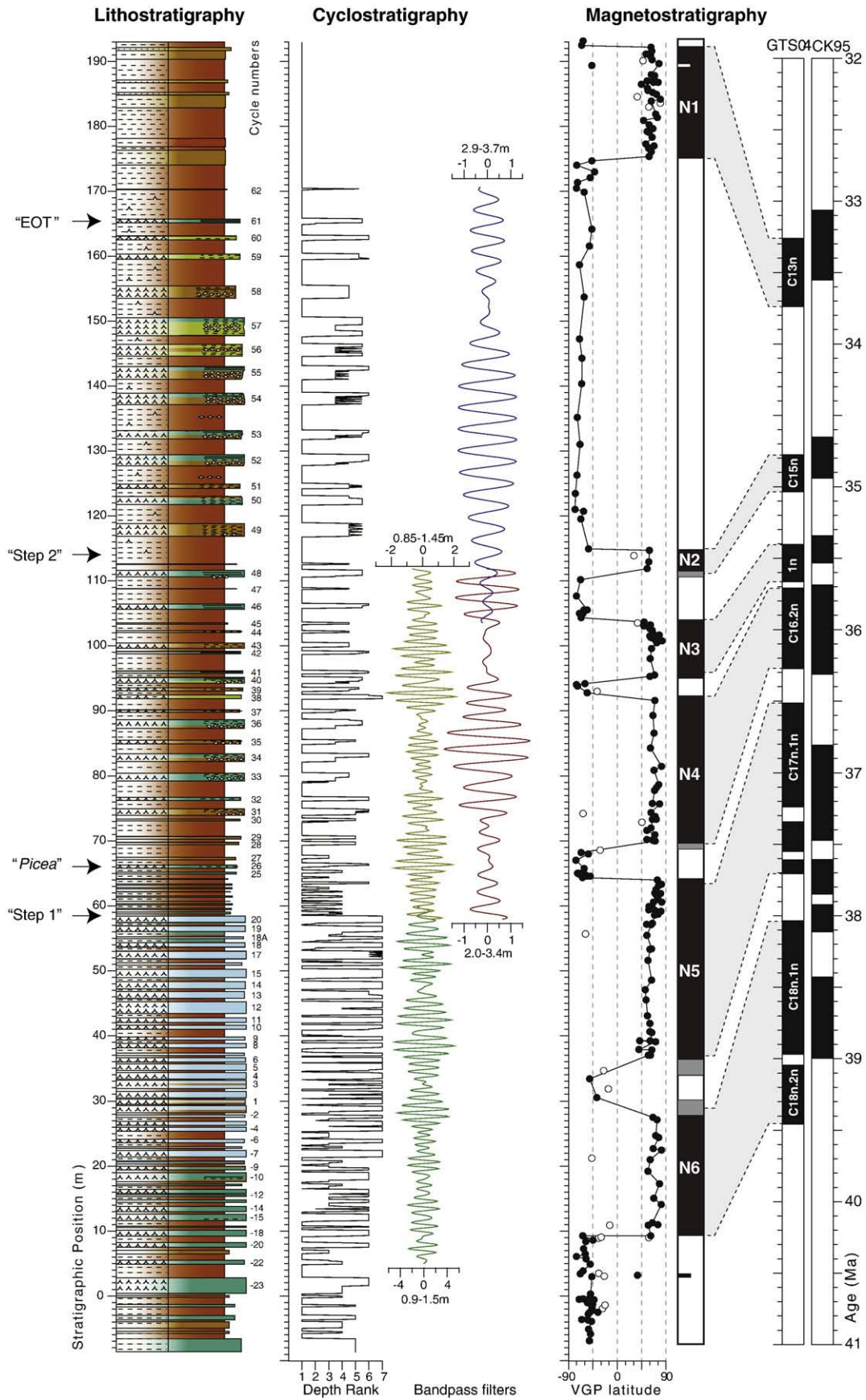


Fig. 3. Simplified basic mudstone–gypsum cycles for the lower part (A), below meter 58, and the upper part (B) of the Shuiwan section depicting the change from thin cycles dominated by massive gypsum beds (A) to thicker cycles dominated by red mudstones and showing laminated, mostly mud-rich reddish-brown gypsum beds (B). Amount of extension of beds to the right in the figure indicate relative degree of induration.

such as rank 4.5 for 'spaced' laminated reddish-brown gypsum, and 5.5 for 'spaced' laminated greyish-green gypsum. Note that the specific gypsum type and associated rank of a specific point does not

significantly affect results of the time series analyses as the time series are dominated by the switches from red bed (rank 1) to gypsum bed (mostly ranks 4 to 7). Redfit power spectra were constructed with the



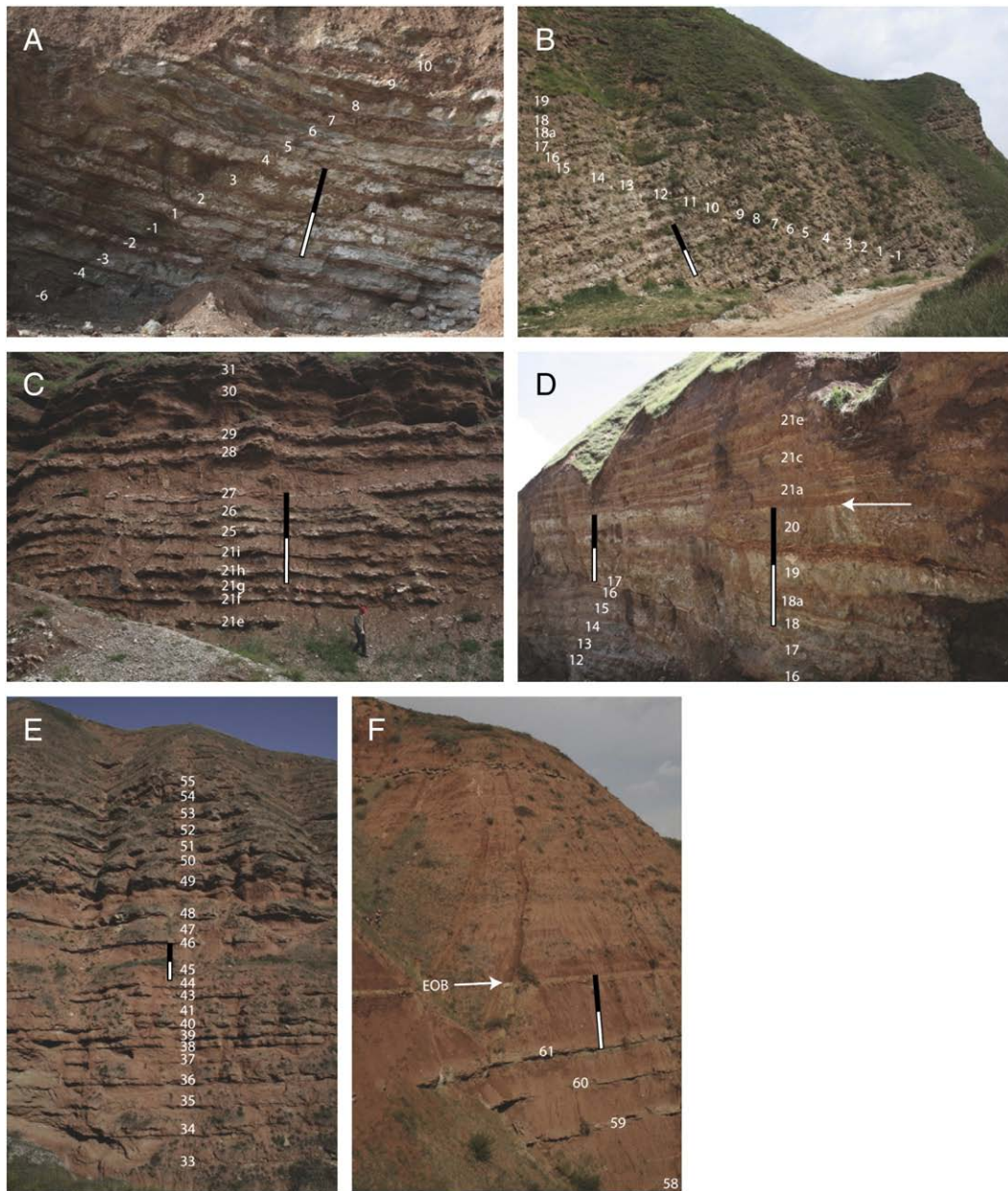


Fig. 5. Photographs of different intervals of the Shuiwan section with small-scale cycle numbers referring the respective position within the section (see Fig. 4 for locating the cycles). Black-white bar represents 5 m in stratigraphy at the location where it is shown in the photo. White arrow in D is the location of the first lithofacies and paleoenvironmental change, while the arrow in F represents the approximate location of the Eocene-Oligocene boundary (EOB).

REDFIT software of Schulz and Mudelsee (2002). Bandpass filtering is performed using Analyseries 1.1 program of Paillard et al. (1996).

3.2.1. Lower interval – cycles –23 to 20

This interval comprises approximately the lower 70 m of the section and is characterised by relatively thin basic cycles of around 1 m as described above in Section 3.1.5 (Figs. 4, 3A, and 2E). The first half of this lower interval is characterised by slightly thicker mudstone intervals within the basic cycles that show nodular, laminated, or massive gypsum beds. After cycle –8 mudstone layers are thinner while gypsum beds are mostly nodular, massive in

character. The observation of this change is slightly hampered by an approximately coeval shift from weathered natural outcrops to freshly excavated quarry outcrops.

Spectral analysis of the depth rank series of this interval indicates a dominant cycle of ~1.3 m in thickness (Fig. 6A). Bandpass filtering of this cycle indicates that this frequency is consistent between cycles –20 to cycle 20 and relates to the basic mudstone–gypsum cyclicity. Other scales of cyclicity are not evident in the power spectra of this interval. In the field, it has been observed that every second or third gypsum bed is less developed (and in some cases not developed resulting in a thicker mudstone). The less developed beds are 18A, 16,

Fig. 4. Lithological column of the Shuiwan section showing lithology, bed colour, induration, sedimentary features, and arbitrarily labelled small-scale cycle numbers. If preferred, the reader is referred to the digital version of the figure in order to be able to zoom in and see details of the column. In the middle, the depth rank series with rank 1 for red mud and ranks 4 to 7 for laminated to massive gypsum beds, see text for detailed explanation on coding, and bandpass filters of the depth rank series for the basic cyclicity in particular stratigraphic intervals. To the right, the VGP latitude is given with interpreted paleomagnetic polarity and finally the correlations to the GTS04 (Gradstein et al., 2004) and CK95 (Cande and Kent, 1995) time scales are given.

13, between 11 and 12, between 9 and 10, 7, 3, 1, -2, -5, -8, -11, -13, -16 (Fig. 4). This results in 14 less well-developed and less-indurated beds within a total of 39 basic cycles, giving a ratio of 1:2.8.

3.2.2. Upper interval – cycles >20 to 61

This interval ranges from meter 58 to meter 170 in the Shuiwan section (Figs. 4, 5E and F), up to cycle 61 which corresponds to the last intercalated gypsum bed in the stratigraphy (Fig. 5F). For this interval, the basic cycle is described in Section 3.1.5 (Fig. 3B) that is characterised by much thicker mudstone with respect to gypsum intervals. The lower half of this interval until around cycle 48 is characterised by a mix of thick and thin basic cycles and accordingly seems to display a less regular cyclicity than in the lower interval discussed in Section 3.2.1 (Fig. 5C and D). Above cycle 48, basic cycle thicknesses become constant around 3 m. The latter cyclicity has been studied in detail by Xiao et al. (2010) using proxy records from the nearby and parallel Tashan section and was interpreted as forced by climate variations related to the 41-kyr obliquity cycle.

Clearer power spectra of the depth rank series were obtained when the two apparently different parts were analysed separately (Fig. 6B and C). The lower part of the upper interval, between cycles 21 and 48, is characterised by two significant spectral peaks averaging in the different spectra at a periodicity between 0.85 and 1.45 m and between 2.0 and 3.4 m, respectively (Fig. 6B and C). Bandpass filtering of these peaks indicates that the shorter peak corresponds to the short-period cyclicity (e.g. cycles 30 to 32 and 38 to 41), and the longer peak corresponds to the long-period cyclicity (e.g. cycles 32 to 37 and 43 to 48). For the interval above cycle 48, the spectra reveal consistent power between 3 and 6 m. For the bandpass filtering, we chose to follow the study by Xiao et al. (2010) as they integrated data from three parallel sections in the Xining Basin as well as all available age estimates for this interval. They found a rather stable periodicity in this interval of around 3.4 m in thickness, which corresponds to the shorter part of the power found here and which we filtered in Fig. 4.

3.3. Isotope stratigraphy

The oxygen and sulphur isotope ratio has been measured on gypsum samples through the Shuiwan section, in order to unravel possible different gypsum sources through time and check for evaporation state of the playa lakes.

3.3.1. Isotope methodology

A total of 44 samples of the freshest possible gypsum sediment have been selected for isotope measurements throughout the section. For each sample about 0.2 g of gypsum material was finely crushed in an agate mortar, dissolved in 100 ml distilled water, and kept at rest for at least 12 h to let precipitate any possible siliciclastic material. 50 ml of the solution was acidified to pH 2 with a 3.33% HCl-solution. The samples were heated to boiling and, upon cooling, 20 ml of 0.25 M BaCl₂-solution was added. The BaSO₄ precipitate was filtered, washed with distilled water, and dried for 12 h at 120 °C. Afterwards 0.2 mg of material was weighted into a silver-foil cup and tightly folded to minimize trapped air. Sulphur stable isotopes were measured on a Fisons NA5100 Elemental Analyser equipped with a teflon sulphur kit. This was connected to a Thermo Delta plus. The conflow interface was omitted and SO₂ reference gas pulses were added via a Dual Inlet. Oxygen stable isotopes were measured on a Thermo TC/EA coupled to a Delta plus. For the measurements, NBS-127 is used as a standard with a measuring precision in these series of 0.5‰ for sulphur isotopes and 0.25‰ for oxygen though slightly increasing upwards in the section due to measurement problems.

3.3.2. Sulphur and oxygen isotopes

The δ³⁴S (VCDT) values of gypsum in the Shuiwan section are between 8‰ and 12‰, with an average of 9.8‰, and a standard

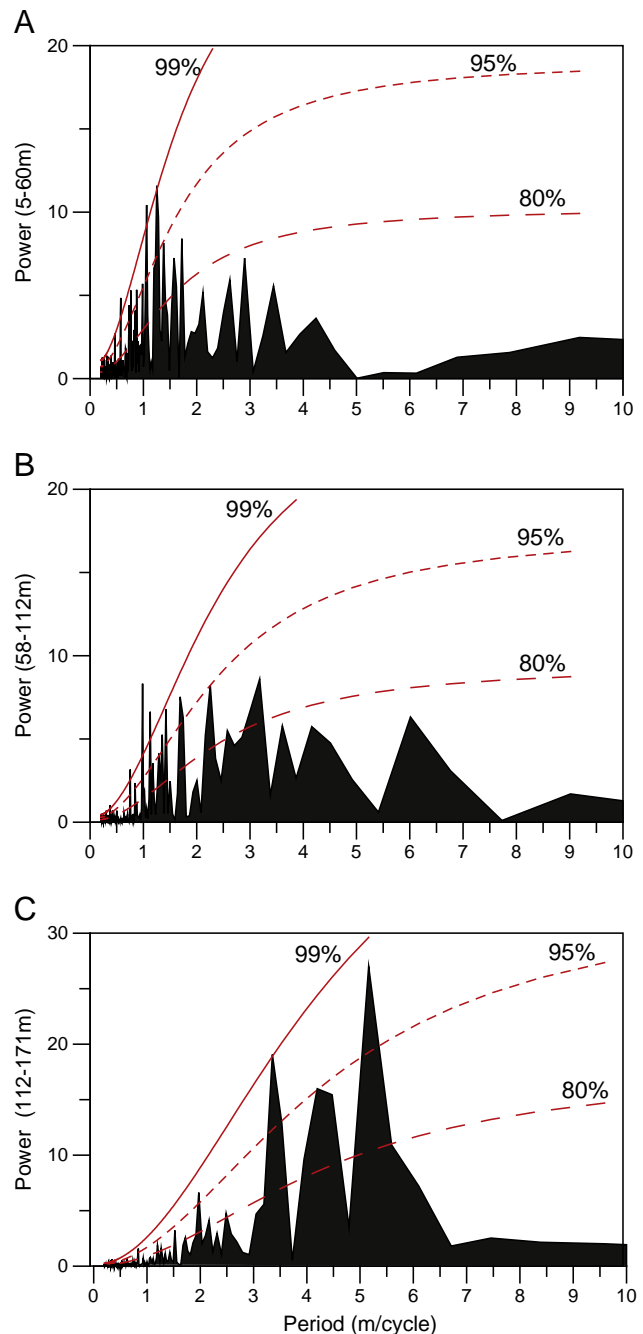


Fig. 6. Power spectra calculated with the Redfit-software from Schulz and Mudelsee (2002). Red-noise boundaries are calculated as upper 80%, 95% and 99% chi-squared limits of a fitted AR1 process. A is for the lower stratigraphic interval from 5 to 60 m, B for the interval from 58 to 112 m, and C from 112 to 171 m.

deviation of 0.9‰ (Fig. 7A). There is no significant trend through the stratigraphy of the Shuiwan section. The δ¹⁸O (SO₄) (VSMOV) values of gypsum samples in the Shuiwan section show roughly similar values through the section ranging between 8.5 and 12‰ with an average of 10.2‰ and a standard deviation of 0.8‰ (Fig. 7A). Similar to the sulphur isotopes, there is no trend present through the section, though the highest values above 11‰ exclusively occur in the lower half of the section. Oxygen (SO₄) and sulphur isotopes plotted against each other reveal no significant trend either (Fig. 7B) and again the lower part of the Shuiwan section (in red) is not distinguishable from the upper part.

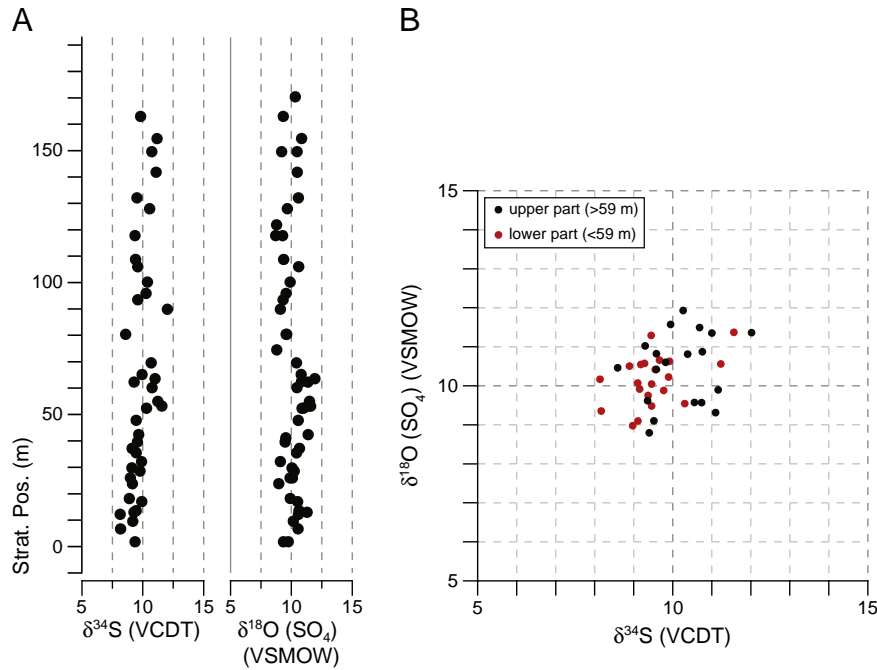


Fig. 7. A) Sulphur and oxygen stable isotope results of sulphate in gypsum samples from the Shuiwan section plotted against stratigraphic position, and B) plotted against each other with red (black) dots for the lower (upper) interval of the section, below (above) 59 m, at the first observed lithofacies and paleoenvironmental change.

The obtained gypsum isotope values are remarkably similar through the section both for oxygen and for sulphur, while the values are thought to reflect the original isotope signal because exchange rates between O of water and O of dissolved sulphate are extremely slow (Lu et al., 2001). The stable sulphur isotopes signature of the Shuiwan section suggests a large stable and homogeneous non-marine source for gypsum solutes throughout the succession as Cenozoic marine sulphur values are all above 17‰ and Late Eocene values around 22‰ (Lu et al., 2001; Paytan et al., 1998; Tan et al., 2006). This means that the observed lithofacies changes are not related to sudden changes in the source of solutes. Nevertheless, also the availability of the same or a similar source can be different through time during deposition of the succession. Furthermore, the very stable and similar values through the section indicate that there was not a long trajectory of gypsum dissolution and reprecipitation from the playa lake margin into deeper parts as then successively heavier sulphur and oxygen (SO₄) values are expected, due to the fractionation during gypsum crystallization of 1.65‰ for δ³⁴S and 3.5‰ for δ¹⁸O (SO₄) (Gibert et al., 2007; Lu et al., 2001).

3.4. Magnetostratigraphy

The results from a previous magnetostratigraphic study of the Shuiwan section (Dupont-Nivet et al., 2007) are supplemented here by higher resolution magnetostratigraphic sampling to better resolve the reversal pattern. Sampling was also extended downwards, in order to check the age of the base of the section that previously relied on correlation to the magnetostratigraphic results of Dai et al. (2006) from the Xiejia section located 15 km away.

3.4.1. Paleomagnetic analysis

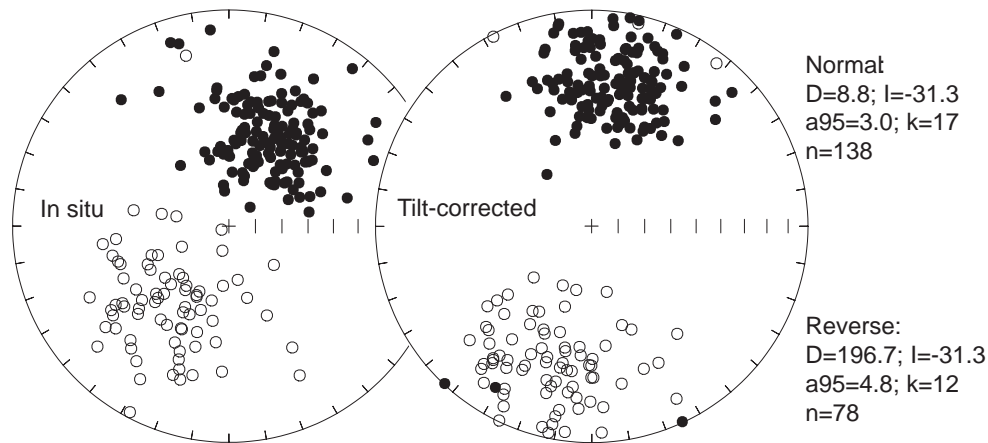
Paleomagnetic sampling was performed using a standard portable coring device. Stepwise thermal demagnetization at up to 19 steps and remanence measurements were performed in a magnetically shielded oven and a 2G 755DC cryogenic magnetometer at Utrecht University Paleomagnetic Laboratory “Fort Hoofddijk.” Pilot samples demagnetized using alternating field treatment yielded less reliable

results than thermal demagnetization that was therefore used for all further samples. Excellent characteristic demagnetization behaviours are identical to previously described results (Dai et al., 2006; Dupont-Nivet et al., 2007; Xiao et al., 2010). After removal of a low temperature component below 250 °C, characteristic remanent magnetization (ChRM) directions decay linearly reaching the origin at ~600 to 620 °C suggesting mostly magnetite as being the main magnetic carriers (see Dai et al., 2006 for rock magnetic analysis). Further linear decay until 670 °C observed on a few samples suggests the combined presence of magnetite and hematite. The ChRM directions were assessed on vector end point diagrams and calculated using least square line analysis (Kirschvink, 1980) estimating the maximum angular deviation (MAD) on a minimum of four measurements. Great circle ChRM analysis (McFadden and McElhinny, 1988) was performed for 8 samples without linear decay but clear demagnetization path along a great circle. Most ChRM directions have MAD below 15°. A few samples showing erratic demagnetization behaviour resulting in ChRM directions with a MAD above 30° were rejected for further analysis (Table S1). Virtual Geomagnetic Pole latitudes (VGP lat.) were calculated from the remaining 238 ChRM directions. To remove outliers and transitional directions, we further rejected 23 ChRM directions with Virtual Geomagnetic Poles (VGP) more than 45° from the mean normal and reverse VGP, respectively. The remaining ChRM directions cluster in antipodal direction after correction of bedding tilt (Fig. 8A). The applied reversals test (Tauxe, 1998) is positive at the 95% confidence level (Fig. 8B) confirming a primary magnetization throughout the record suitable for the construction of the magnetostratigraphy. Seven reversed (R1–R7) and six normal (N1–N6) polarity zones were defined based on at least two successive VGP directions of the same polarity thus discarding two isolated VGP directions (Fig. 4).

3.4.2. Correlation to the GPTS

The obtained pattern is similar to that previously found in the same stratigraphic interval in the Xiejia and Tashan sections with two important differences (Dupont-Nivet et al., 2007; Xiao et al., 2010). The first of these is that we do not find a short reversed interval in R1

A. ChRM directions



B. Positive reversals test

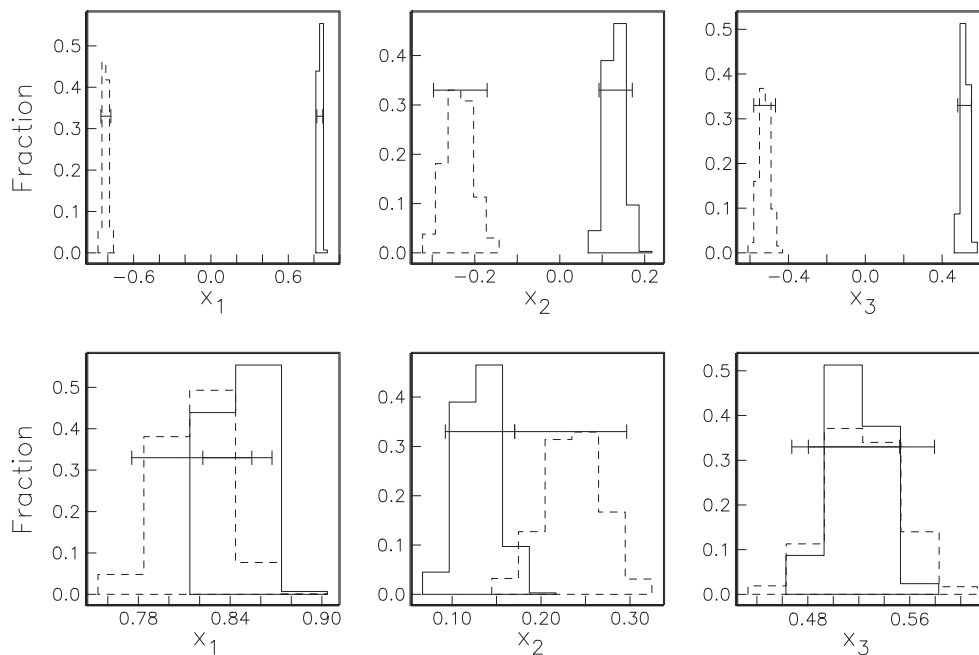


Fig. 8. A) Equal-area projections of characteristic remanent magnetization (ChRM) directions from the Shuiwan section before and after tilt correction (downward (upward) directions are shown as solid (open) circles). B) These data define positive reversals tests with the mean normal direction being antipodal within 95% confidence to the mean reverse direction (Tauxe, 1998).

which is reported from the Tashan section (Xiao et al., 2010). This short interval is suggested to result either from recording of a cryptochron in C13n or from unreliable directions in a gypsiferous interval. The latter hypothesis seems more appropriate in light of our high-resolution results showing exclusively normal polarity directions in that interval in the Shuiwan section. The second and most important difference is that we find a new long normal zone (N6) in the extension of the base of the section that is not reported in the parallel Xiejia section (Dai et al., 2006). This requires changing the previously proposed age model for the lower part of the section (Dai et al., 2006; Dupont-Nivet et al., 2007, 2008).

Clearly now, the base of N5 has to be correlated to the base of C17n and the base of N6 to the base of C18n (Fig. 4). The resulting pattern is also in better agreement with the correlation of N2 and N3 to C15n and C16n respectively, without requiring missing C16r.1r (Dupont-Nivet et al., 2007). Finally, our results imply that polarity zone N6 has been missed in the Xiejia record, which might be related to faulting in that rather disturbed part of the Xiejia section. Despite higher sampling resolution, still the shortest chrons in the sampled interval

(C17n.1r = 131 kyr; C17n.2r = 72 kyr; C18n.1r = 79 kyr) have not been detected (Fig. 4). The low accumulation rates (~2 cm/kyr) and the occurrence of gypsum intervals yielding no paleomagnetic signal can explain the absence of these short intervals in addition to the possibility of short gaps in the stratigraphic record.

3.4.3. Age model and sedimentation rates

We used both the time scale of Cande and Kent (1995) (hereafter CK95) and Gradstein et al. (2004) (hereafter GTS04) in order to calculate the sedimentation rates through the Shuiwan section. The recalibration of ignimbrite ages of New Mexico (McIntosh et al., 1992) using astronomical intercalibrated age for the FCT of 28.201 ± 0.022 Ma of Kuiper et al. (2008) or the revised Fish Canyon Tuff age of 28.02 ± 0.28 Ma of Renne et al. (1998), indicates that the CK95 time scale (Cande and Kent, 1995) is not far off the revised radiometric dates for the Eocene–Oligocene boundary, the top of C15n, and the top of C17n.1n (see Hilgen and Kuiper, 2009). At present, no reliable absolute time scale for the Late Eocene exists based on astronomical tuning. Astronomical constraints for duration of Late Eocene chrons (Pälike et al., 2001) result

in similar duration for C17n (1n–3n) with respect to CK95 (1.493 and 1.495 Myr respectively), which is slightly longer than GTS04 (1.259 Myr), and similar duration for C16n (1n–2n) with respect to GTS04 (0.866 and 0.872 Myr respectively), which is slightly shorter than in CK95 (0.998 Myr). Based on these comparisons, we decided to use both the CK95 and GTS04 time scales, in order to investigate the long-term sedimentation rates in the Shuiwan section.

The sedimentation rates show a clear increase from bottom to top of the section (Fig. 9). Remarkably, the increase in sedimentation rates occurs in two steps; the first step around the base of C16n.2n is less prominent than the second more pronounced step near the top of chron C15n. Average sedimentation rates for these intervals, which we calculated from both time scales, increase from ~21 m/Myr to ~28 m/Myr at the first step and to ~46 m/Myr at the second step. Both steps fit with lithofacies and lithostratigraphic changes described above as well as the high-altitude pollen appearance at the first step.

3.5. Cyclostratigraphy

Field observations and time series analysis of the depth rank series (see Sections 3.2.1 and 4.2.2) indicate increasing thickness of the mudstone–gypsum cyclicity upward in the section (Figs. 4 and 6). Using the established age model, durations for the cyclicity can be calculated and compared to durations of orbital cycles that potentially drove the lithological cyclicity. In the lower part of the section, the 1.2 m thick mudstone–gypsum cycles have durations of around 55 kyr according to the GTS04 time scale (48 kyr in CK95). In the middle part of the section, between the first and the second increases in sedimentation rate, the 1.1 m cyclicity has a duration of around 37 kyr according to the GTS04 time scale (42 kyr in CK95), while the 2.5 m cyclicity a duration of approximately 82 kyr (93 kyr in CK95). For the upper interval, between the second increase in sedimentation rate and the EOT, the basic cycle thickness of 3.2 m (close to the 3.4 m found by Xiao et al., 2010) implies an average duration of ~55 kyr in GTS04 (~59 kyr in CK95) using C13r sedimentation rates.

Xiao et al. (2010) have been thoroughly investigating the cyclicity in chron C13r including examination of existing time scales. They concluded that the most likely driving mechanism behind the basic cyclicity in this interval is orbital forcing of climate by the 41-kyr

obliquity cycle. Our cyclostratigraphic analysis and magnetostratigraphic age control indicates that the basic cyclicity in the parts below chron C13r also have a duration close to the duration of obliquity. Astronomical forcing is suggested as driving mechanism of the basic cyclicity by the strong regularity of mudstone–gypsum cycles (Figs. 5A, B, and D, and 4). In the interval below cycle 20, apart from the basic cyclicity another scale of cyclicity has been observed in outcrop occurring at a ratio of 1:2.8 (see Section 3.2.1). Above cycle 20, basic cycles display a ratio of 1:2.23 and are interpreted as a mix of two periodicities. Based on these observations, we argue that the basic cyclicity in the whole Shuiwan section is likely forced by the 41-kyr obliquity cycle. The other scale of cyclicity in the intervals between cycles –20 and 20 and between cycles 20 and 48 with periods of 112 and 92 kyr, respectively, are then in the range of the ~100-kyr period of short eccentricity (Fig. 4).

4. Discussion

Our integrated stratigraphic and sedimentologic data from the Xining Basin reveal two stepwise paleoenvironmental changes preceding the Eocene–Oligocene Transition (EOT) and a dominance of obliquity-forcing in driving lithological cyclicity in the entire upper Eocene. Below, we discuss the paleoenvironmental significance of our findings and place them within a regional and global perspective.

4.1. Late Eocene paleoenvironmental deterioration

4.1.1. First step at the top of C17n.1n (~36.6 Ma)

The first step occurs in the top of chron C17n.1n at ~36.6 Ma according to the GTS04 (~36.9 Ma in CK95). It shows a decrease in gypsum content relative to mudstone and a shift to less stable saline lake systems indicated by a change in the gypsum facies (Fig. 4; Sections 3.1.5 and 3.2). These changes are interpreted here as a decrease in water availability with gypsum facies being the relatively wettest equivalent within the mudstone–gypsum packages (see Section 3.1.6). The slight change in sedimentation rate observed from the magnetostratigraphic age model (Fig. 9) disappears if sedimentation rates are derived assuming obliquity forcing of basic cyclicity that has nearly similar thickness on both sides of the

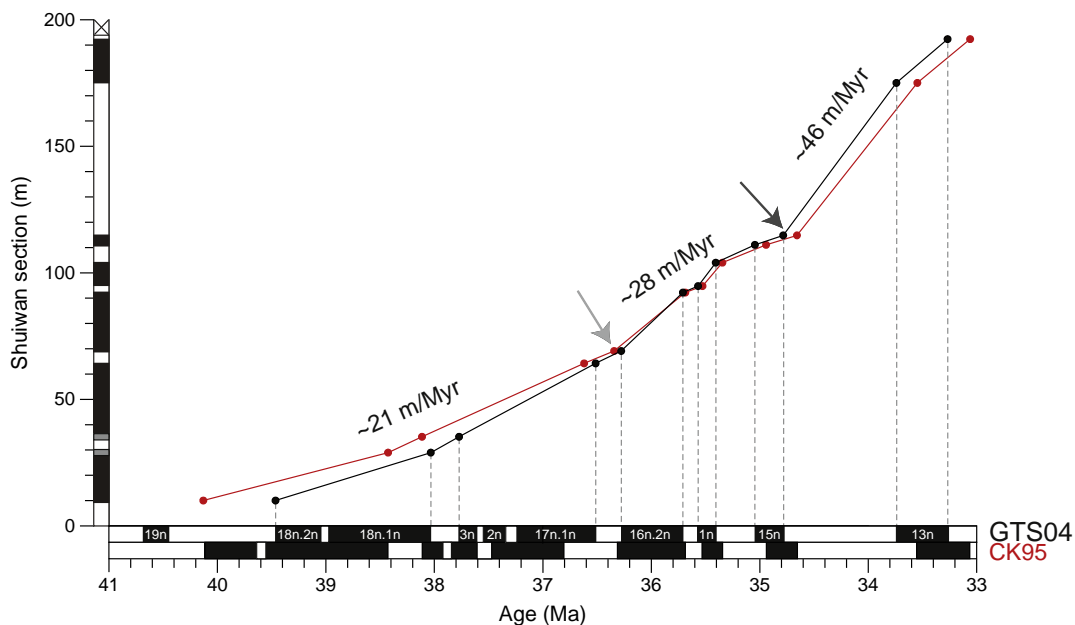


Fig. 9. Sedimentation rate plots for the Shuiwan section using the GTS04 (Gradstein et al., 2004) time scale in black and the CK95 (Cande and Kent, 1995) time scale in red. Average sedimentation rates for approximately stable intervals are given between locations of apparent sudden change (increase) in sedimentation rates indicated by grey arrows.

lithofacies change. In the parallel Xiejia section, located approximately 15 km to the south, a similar lithofacies change occurs time-equivalent indicating the regional character of the change (data not shown here; Dupont-Nivet et al., 2007). Therefore, the first shift is interpreted as a regional aridification in line with interpretations of similar changes observed at the Eocene–Oligocene Transition (Dupont-Nivet et al., 2007; Xiao et al., 2010).

This regional aridification at ~36.6 occurs close to the high-altitude pollen appearance (Dupont-Nivet et al., 2008; Hoorn et al., 2010) that is now dated more precisely in chron C16.2r at ~36.4 Ma. The sudden appearance of the Pinaceae family, and in particular that of taxon *Picea* (*Piceapollenites*), has been interpreted as reaching threshold conditions for vegetation change after the long-term combined effects of regional uplift and gradual global cooling, rather than several kilometers of uplift within such a short time span. Indeed, the close simultaneity of the paleoenvironmental change shown by our data with the rather sudden pollen appearance strongly suggests threshold conditions for the appearance were constrained by regional paleoclimate, while on the long term uplift caused the appearance of the high altitude habitats. Our data indicate a time lag of around 0.2 million years between the lithofacies step and the high altitude pollen appearance. Interestingly, this takes place within a peculiar interval (between cycles 20 and 25, Fig. 4) where several thin cycles occur at a scale that would typically be in the precession-band with bundles occurring at 100-kyr eccentricity level (see Fig. 5C and D). Also, in the middle of this interval, we found the only gypsarenite in the entire section, indicative of surface transport and reworking of gypsum. Apparently, this interval reflects a transitional period between the stable characteristics below and above. This suggests that during the transitional period, local depositional environments reacted before the regional pollen habitats accommodated to changes in external, possibly global, forcing.

4.1.2. Second step in the base of chron C13r (~34.7 Ma)

The second change in the Shuiwan section occurs at ~34.7 Ma in the base of chron C13r. Here, a clear increase in sedimentation rates is observed from ~28 m/Myr to ~46 m/Myr (Fig. 9). Interestingly, this stepwise increase in sedimentation rates can be associated with considerable increase in mudstone interval thicknesses while the gypsum intervals remain relatively constant in thickness. Considering the steady duration of around 41 kyr for the basic mudstone–gypsum cycles, this implies that the observed enhanced sedimentation rate above cycle 48 is related to higher accumulation of siliciclastic material and not of gypsum.

Enhanced aggradation can be linked to increased subsidence facilitating accommodation space, though we argue that this is not likely here. First, tectonic changes are not expected to be step-wise although tectonic–climate interactions might hide a gradual tectonic change. Second, sedimentation rates decreases after the EOT implying only a 1 million year interval of possible increased subsidence rates, which is not expected from a tectonic origin. Third, sedimentary patterns indicate an underfilled state of the basin during Eocene and Oligocene times which implies that subsidence rates do not control accumulation rates at relatively short time scales.

Other explanations for the large increase in clastic accumulation are more likely. It can be linked to lower deflation rates at the depositional site due to lower wind erosion of the saline mudflats (Shaw and Thomas, 1989). Or, intensification of the transport mechanism may also explain higher clastic input, however, this cannot be further assessed since it is not known whether wind, water, or a combination of both were the dominant media of transport. Finally, enhanced production and availability of clastic material in the source areas may be an important mechanism as well. It may relate to increased seasonal differences and/or increased aridity leading to higher physical over chemical weathering or, alternatively, to partial disappearance of the protective vegetation cover (Scoging, 1989).

Clearly, the transport mechanism(s) and source(s) of clastic material need to be further investigated in order to give a paleoenvironmental interpretation to the observed increased accumulation rates at ~34.7 Ma in the Shuiwan section. In light of the documented aridification at the first step at ~36.6 Ma and at the EOT at ~34 Ma, we may tentatively similarly interpret the increased sedimentation rate as a result of aridification with decrease of protective cover at the basin margin and increases in production of clastic material and input of clastic material by wind transport.

Some similarities of our studied interval with the time preceding the major Northern Hemisphere glaciations at ~3–4 Ma suggests a tentative comparison here. At that time, global records indicate sudden multiple increases in sedimentation rates which have suggested to be related to climatic instability leading to disequilibrium in fluvial and glacial landscapes which in turn invoked high weathering rates (Zhang et al., 2001). In the interval directly preceding the Eocene–Oligocene Transition, a relatively unstable climate can be expected as ephemeral ice sheets on the Southern Hemisphere were growing likely with a strong obliquity-dominated pacing (Xiao et al., 2010). This might have led to large differences between warm and wet and cold and dry stages preventing landscapes surrounding the Xining Basin to reach equilibrium state and thus invoking rapid weathering.

4.1.3. Late Eocene obliquity forcing

Our cyclostratigraphic investigations indicate that dominant 41-kyr obliquity forcing extends from the entire Late Eocene interval present in the Shuiwan section starting at ~39.5 Ma at the base of chron C18n.2n and ending at the Eocene–Oligocene Transition (EOT). Apart from the obliquity forcing, additional imprint of the short 100-kyr eccentricity cycle is found, especially in the middle interval between the first and second paleoenvironmental steps at ~36.6 Ma to ~34.7 Ma, and to a lesser extent in the interval below 36.6 Ma. However, obliquity was apparently the dominant forcing mechanism leading to almost 6 million of years with recurrent periods during which net water availability allowed for gypsum precipitation. These results are robust for existing time scales proposed for this period but ultimate confirmation will be possible when astronomically-calibrated absolute time scales are available for the Late Eocene.

The occurrence of Late Eocene obliquity forcing in marine and continental records and the possible origin of obliquity forcing within the latest Eocene Xining Basin record has been discussed extensively by Xiao et al. (2010). They argued that the strong obliquity cyclicity observed in the Xining Basin, outside an interval with low eccentricity values related to the 2.4-Myr eccentricity cycle, is caused by high-latitude ice volume variability influencing climate over central Asia at this time. In line with previous hypotheses, they further suggested this might be related to incipient ice sheets that are highly susceptible to environmental and climatological changes, and that might have a significant impact on global climate due to their presence–absence behaviour (Pälike et al., 2001; Westerhold and Röhl, 2009; Xiao et al., 2010). Here, we follow these hypotheses, which seem to be valid for the period extending from the base of chron C18n ~39 Ma until the EOT at ~34 Ma for paleoenvironments and sedimentation in the Xining Basin.

Further insight on the effect of obliquity on Asian continental interior climates comes from an Eocene model experiment by Lawrence et al. (2003) in which maximal seasonal contrast is depicted by changing both obliquity and precession. This study shows that the seasonal contrast changes significantly between obliquity extremes. In particular, annual precipitation over the continental interior increases by 11 to 18% during periods of maximal seasonal contrast and so likely as well during obliquity maxima. Lawrence et al. (2003) state that the exact value at a certain point highly depends on local topography, though the general trends of precipitation in central Asia are clear from their results. Therefore, saline lake extensions in the Xining Basin most likely took place during obliquity maxima.

4.2. Comparison with regional and global records

Cenozoic Asian paleoenvironmental changes are usually associated to regional uplift of the Tibetan plateau. In the case of the Xining Basin, there is certainly a long-term tectonic/orographic effect affecting the paleoenvironments as expressed by the appearance of high-altitude pollen. However, the obliquity forcing, the record of the EOT and the abrupt character of the two observed paleoenvironmental steps indicate the basin dynamics responded to global climate change as well during late Eocene to Oligocene times. Particularly robust is the first paleoenvironmental change we observe in the top of chron C17n.1n at ~36.6 Ma indicating aridification of western Chinese climate. Therefore, it is likely that this step would also be found in other records, either regionally or globally. In the continental interior of Asia, existing paleoenvironmental and biostratigraphic records indeed indicate aridification and cooling north of the Tibetan plateau in agreement with our results (Graham et al., 2005; Kraatz and Geisler, 2010; Meng and McKenna, 1998; Sun and Wang, 2005). Unfortunately, these records are not dated with sufficient accuracy for regional correlations with the Xining Basin records. Bosboom et al. (2011) recently constrained the final major retreat of the shallow epicontinental sea out of the Tarim Basin to an early Priabonian age ~37 Ma (overlap between dinoflagellate Mps Interval Zone and calcareous nannofossil zone CP14). Climate model experiments showed that the retreat of this inland sea, which was a prominent moisture source for the Xining area during the Eocene, drastically reduces moisture transport to the Xining Basin especially in winter (Ramstein et al., 1997; Zhang et al., 2007). This mechanism and the close age relationship suggest a connection between this newly-dated retreat of the Tarim sea at ~37 Ma and the regional aridification step in the Xining Basin at ~36.6 Ma. Both of these abrupt changes could then have, apart from long term regional (tectonic) trends, a global origin, likely to be cooling and ice volume increase, as a step towards the Eocene–Oligocene Transition (EOT).

Global changes have been reported that are coeval to the first step observed in our records. Well-dated oxygen isotope records along this interval of time are still scarce but available records show indications for two small cooling events (Carbonate Accumulation Event 5 (CAE5) and cooling event C) found approximately in the top of chron C17n.1n (Lyle et al., 2005; Villa et al., 2008). We may speculate that, even though these cooling events and ice growth steps were small, when threshold conditions in the Tarim sea and/or in the Xining Basin were close to being reached, these might have been the trigger for causing the observed changes. However, still much of the global paleoclimate history of this interval of time is to be resolved and especially also accurately dated before these speculations can be validated. More conclusively, in the top of chron C17n.1n at ~36.6 Ma (GTS04), Pälike et al. (2001) report an apparent change in the dominance of orbitally-driven changes from climatic precession to obliquity in marine sediments from Blake Nose in the Atlantic. They interpret this as being related to changes in the ocean circulation system and the dominant climatic regime, as the timing seem to be approximately consistent with the appearance of ice sheets at high latitude (Pälike et al., 2001). Another coeval global change, albeit much less well-dated, is reported globally at the Bartonian–Priabonian boundary that corresponds to a widespread sea-level lowstand and is frequently marked by a hiatus separating it from the Priabonian (Gradstein et al., 2004). Therefore, the hypothesis formulated by Dupont-Nivet et al. (2007) for the Eocene–Oligocene Transition may be valid for this older step as well. This is, global cooling and/or (Antarctic) ice volume increase and concurrent sea-level lowering leading to sea retreat from the Tarim Basin and finally to aridification in the Xining Basin area by decreasing moisture supply.

The second step in the base of chron C13r at ~34.7 Ma has less potential coeval global changes reported in literature. The most likely candidate is the so-called 'Vanhof cooling event' that is roughly dated

between 35 and 35.5 Ma (Bohaty and Zachos, 2003; Vanhof et al., 2000). This is a rather abrupt cooling event that occurs on the gradual latest Eocene cooling trend that culminates in the EOT at ~34 Ma. Eldrett et al. (2007) document a cooling of 5–6 °C in cold-month (winter) mean temperatures to 0–2 °C, and a concomitant increased seasonality before the EOT. Although it is hard to exactly pinpoint the start of this change, it seems to have occurred before or in the base of chron C13r (ODP Site 643A data), which thus would match with our paleoenvironmental step at this time. Increased seasonality might have been the mechanism that led to enhanced clastic supply to the Xining area at this step. Here, we should be careful as the paleoenvironmental interpretation of our Chinese record needs further detailed sedimentological investigation in order to better understand the accumulation of clastic material in the Xining Basin.

5. Conclusions

Two step-wise paleoenvironmental changes are observed in the continental sediment records from the Xining Basin, China, in the Late Eocene climatic 'doubthouse' period preceding the Eocene–Oligocene Transition at 34 Ma. The first step occurs in the top of chron C17n.1n at ~36.6 Ma and suggests a regional aridification. This step can now be linked to a coeval retreat of the Tarim Sea recently dated as early Priabonian. The near synchrony of these events with a change from precession to obliquity domination in the Atlantic Ocean and with the less well-dated Bartonian–Priabonian sea-level low-stand suggests a global origin. The second step occurs in the base of chron C13r at ~34.7 Ma and reveals a significant clastic sedimentation rate increase. A reported increase in high-latitude seasonality around this time might have been the cause of this (seasonal) drying trend. Decreased climate stability preceding the greenhouse to icehouse transition at the EOT might have prevented landscapes to attain equilibrium configurations. Cyclostratigraphic analysis indicates that cyclicity in the whole studied record is dominantly driven by the 41-kyr obliquity cycle with minor impact of short ~100-kyr eccentricity before ~34.7 Ma. From this, we interpret that the Xining Basin paleoenvironments were very sensitive to high-latitude climate change possibly (partly) related to incipient ice sheets causing large amplitude variability in the late Eocene preceding the greenhouse to icehouse transition at the Eocene–Oligocene boundary.

Supplementary materials related to this article can be found online at doi:10.1016/j.palaeo.2010.11.028.

Acknowledgements

H.A. is grateful for funding from the NWO-ALW Vernieuwingsimpuls (VI) of W.K. H.A., G.D.-N., and R.B. acknowledge NWO-ALW and NSFC for funding of research visits and grants. Xiao G. Q. thanks the Foundation of Geological Survey of China (grant no. 1212010610103) for funding. Dai Shuang, Zhuqiang, Huang Wentao, Guo Zhaojie, Wang Yongshen, Ste, Marijke Lebbink, Julia Straathof, Cor Langereis, Carina Hoorn, Frits Hilgen and Jef Vandenberghe are thanked for assistance, advice, and discussions both in and out of the field. Arnold van Dijk is thanked for assistance with preparation and measurements of gypsum isotopes. Laura Rosell and Federico Ortí from the Universitat de Barcelona are thanked for discussions on gypsum facies and stable isotopes. Editor Peter Kershaw, Laura Rosell, and an anonymous reviewer are thanked for their thorough reviews that considerably improved the manuscript.

References

- Abels, H.A., Abdul Aziz, H., Calvo, J.P., Tuenter, E., 2009. Shallow lacustrine microfacies document orbitally paced lake-level history in the Miocene Teruel Basin (NE Spain). *Sedimentology* 56, 399–419.

- Bijl, P.K., Schouten, S., Sluijs, A., Reichert, G.J., Zachos, J.C., Brinkhuis, H., 2009. Early Palaeogene temperature evolution of the southwest Pacific Ocean. *Nature* 461, 776–779.
- Bohaty, S.M., Zachos, J.C., 2003. Significant Southern Ocean warming event in the late middle Eocene. *Geology* 31, 1017–1020.
- Bohaty, S.M., Zachos, J.C., Florindo, F., Delaney, M.L., 2009. Coupled greenhouse warming and deep-sea acidification in the middle Eocene. *Paleoceanography* 24, PA2207. doi:10.1029/2008PA001676.
- Bosboom, R.E., Dupont-Nivet, G., Houben, A.J.P., Brinkhuis, H., Villa, G., Mandic, O., Stoica, M., Zachariasse, W.J., Guo, Z., Li, C., Krijgsman, W., 2011. Late Eocene sea retreat from the Tarim Basin (west China) and concomitant Asian paleoenvironmental change. *Palaeogeogr. Palaeoclimatol. Palaeoecol.* 299, 385–398.
- Cande, S.C., Kent, D.V., 1995. Revised calibration of the geomagnetic polarity timescale for the Late Cretaceous and Cenozoic. *J. Geophys. Res.* 100, 6093–6095.
- Coxall, H.K., Pearson, P.N., 2007. The Eocene–Oligocene transition. In: Williams, M., Haywood, A.M., Gregory, F.J., Schmidt, D.N. (Eds.), *Deep-Time Perspectives on Climate Change: Marrying the Signal from Computer Models and Biological Proxies*. The Micropaleontological Society Special Publications, London, pp. 351–387. Book series, vol.
- Coxall, H.K., Wilson, P.A., Pälike, H., Lear, C.H., Backman, J., 2005. Rapid stepwise onset of Antarctic glaciation and deeper calcite compensation in the Pacific Ocean. *Nature* 433, 53–57.
- Dai, S., Fang, X., Dupont-Nivet, G., Song, C., Gao, J., Krijgsman, W., Langereis, C.G., Zhang, W., 2006. Magnetostratigraphy of Cenozoic sediments from the Xining Basin: tectonic implications for the northeastern Tibetan Plateau. *J. Geophys. Res.* 111, B11102. doi:10.1029/2005JB004187.
- Dupont-Nivet, G., Horton, B.K., Butler, R.F., Wang, J., Zhou, J., Waanders, G.L., 2004. Paleogene clockwise tectonic rotation of the Xining-Lanzhou region, northeastern Tibetan Plateau. *J. Geophys. Res.* 109, B04401. doi:10.1029/2003JB002620.
- Dupont-Nivet, G., Krijgsman, W., Langereis, C.G., Abels, H.A., Dai, S., Fang, X., 2007. Tibetan plateau aridification linked to global cooling at the Eocene–Oligocene transition. *Nature* 445, 635–638.
- Dupont-Nivet, G., Hoorn, C., Konert, M., 2008. Tibetan uplift prior to the Eocene–Oligocene climate transition: evidence from pollen analysis of the Xining Basin. *Geology* 36, 987–990.
- Eldrett, J.S., Harding, I.C., Wilson, P.A., Butler, E., Roberts, A.P., 2007. Continental ice in Greenland during the Eocene and Oligocene. *Nature* 446, 176–179.
- Gibert, L., Ortí, F., Rosell, L., 2007. Plio-Pleistocene lacustrine evaporites of the Baza Basin (Betic Chain, SE Spain). *Sed. Geol.* 200, 89–116.
- Gradstein, F.M., Ogg, J.G., Smith, A.G., 2004. *A Geologic Time Scale 2004*. Cambridge University Press, Cambridge, pp. 1–589.
- Graham, S.A., Chamberlain, C.P., Yue, Y.J., Ritts, B.D., Hanson, A.D., Horton, T.W., Waldbauer, J.R., Poage, M.A., Feng, X., 2005. Stable isotope records of Cenozoic climate and topography, Tibetan Plateau and Tarim Basin. *Am. J. Sci.* 305, 101–118.
- Hilgen, F.J., Kuiper, K.F., 2009. A critical evaluation of the numerical age of the Eocene–Oligocene boundary. In: Koeberl, C., Montanari, A. (Eds.), *The Late Eocene Earth – Hothouse, Icehouse, and Impacts: Geological Society of America Special Paper*, vol. 452, pp. 139–148.
- Hoorn, C., J. Straathof, H. A. Abels and G. Dupont-Nivet, 2010. The Eocene–Oligocene palynological record from the Xining Basin (Tibetan Plateau, China) as evidence for Asian paleoenvironments and regional change. In: (Eds.), *EGU General Assembly 2010: Geophysical Research Abstracts*. Book Series, Vol. 12. Vienna, EGU2010-12388.
- Horton, B.K., Dupont-Nivet, G., Zhou, J., Waanders, G.L., Butler, R.F., Wang, J., 2004. Mesozoic–Cenozoic evolution of the Xining–Minhe and Dangchang basins, northeastern Tibetan Plateau: magnetostratigraphic and biostratigraphic results. *J. Geophys. Res.* 109, B04402. doi:10.1029/2003JB002913.
- Kirschvink, J.L., 1980. The least-squares line and plane and the analysis of paleomagnetic data. *Geophys. J. R. Astr. Soc.* 62, 699–718.
- Kraatz, B.P., Geisler, J.H., 2010. Eocene–Oligocene transition in Central Asia and its effects on mammalian evolution. *Geology* 38, 111–114.
- Kuiper, K.F., Deino, A., Hilgen, F.J., Krijgsman, W., Renne, P.R., Wijbrans, J.R., 2008. Synchronizing rock clocks of earth history. *Science* 320, 500–504.
- Lawrence, K.T., Sloan, L.C., Sewall, J.O., 2003. Terrestrial climatic response to precessional orbital forcing in the Eocene. *Geological Society of America Special Paper*, 369, pp. 65–77.
- Lu, F.H., Meyers, W.J., Schoonen, M.A., 2001. S and O (SO₄) isotopes, simultaneous modeling, and environmental significance of the Nijar messinian gypsum, Spain. *Geochim. Cosmochim. Acta* 65, 3081–3092.
- Lu, H., Wu, N., Yang, X., Shen, C., Zhu, L., Wang, L., Li, Q., Xu, D., Tong, G., Sun, X., 2007. Spatial pattern of Abies and Picea surface pollen distribution along the elevation gradient in the Qinghai–Tibetan Plateau and Xinjiang, China. *Boreas* 37, 254–262.
- Lyle, M., Olivarez Lyle, A., Backman, J., Tripathi, A.K., 2005. Biogenic sedimentation in the Eocene equatorial Pacific – the stuttering greenhouse and Eocene carbonate compensation depth. In: Wilson, P.A., Lyle, M., Firth, J.V. (Eds.), *Proceedings of the Ocean Drilling Program, Scientific Results*, vol. 199, pp. 1–35. Available online: http://www-odp.tamu.edu/publications/199_SR/VOLUME/CHAPTERS/219.PDF.
- Lyle, M., Barron, J., Bralower, T.J., Huber, M., Olivarez Lyle, A., Ravelo, A.C., Rea, D.K., Wilson, P.A., 2008. Pacific ocean and Cenozoic evolution of climate. *Rev. Geophys.* 46 8755–1209/08/2005RG000190.
- McFadden, P.L., McElhinny, M.W., 1988. The combined analysis of remagnetization circles and direct observations in paleomagnetism. *Earth Planet. Sci. Lett.* 87, 161–172.
- McIntosh, W.C., Geissman, J.W., Chapin, C.E., Kunk, M.J., Henry, C.D., 1992. Calibration of the latest Eocene–Oligocene geomagnetic polarity time scale using 40Ar/39Ar dated ignimbrites. *Geology* 20, 459–463.
- Meng, J., McKenna, M.C., 1998. Faunal turnovers of Palaeogene mammals from the Mongolian Plateau. *Nature* 394, 364–367.
- Ortí, F., Rosell, L., Anadón, P., 2003. Deep to shallow lacustrine evaporites in the Libros Gypsum (southern Teruel Basin, Miocene, NE Spain): an occurrence of pelletal gypsum rhythmites. *Sedimentology* 50, 361–386.
- Ortí, F., Rosell, L., Inglès, M., Playà, E., 2007. Depositional models of lacustrine evaporites in the SE margin of the Ebro Basin (Paleogene, NE Spain). *Geol. Acta* 5, 19–34.
- Paillard, D.L., Labeyrie, L., Yiou, P., 1996. Macintosh program performs time-series analysis. *EOS Trans. AGU* 77, 379.
- Pälike, H., Shackleton, N.J., Röhl, U., 2001. Astronomical forcing in Late Eocene marine sediments. *Earth Planet. Sci. Lett.* 193, 589–602.
- Paytan, A., Kastner, M., Campbell, D., Thieme, M.H., 1998. Sulfur isotopic composition of Cenozoic seawater sulfate. *Science* 282, 1459–1462.
- Ramstein, G., Fluteau, F., Besse, J., Joussaume, S., 1997. Effect of orogeny, plate motion and land–sea distribution on Eurasian climate change over the past 30 million years. *Nature* 386, 788–795.
- Renne, P.R., Swisher, C.C., Deino, A.L., Karner, D.B., Owens, T.L., DePaolo, D.J., 1998. Intercalibration of the lower Pleistocene timescale based on ODP Site 677. *Chem. Geol.* 145, 117–152.
- Rosen, M.R., 1994. The importance of groundwater in playas: a review of playa classifications and the sedimentology and hydrology of playas. In: Rosen, M.R. (Ed.), *Paleoclimate and Basin Evolution of Playa Systems*. Geological Society of America, Boulder, Colorado, pp. 1–18. Book series, vol. Special Paper 289.
- Schulz, M., Mudelsee, M., 2002. REDFIT: estimating red-noise spectra directly from unevenly spaced paleoclimatic time series. *Comput. Geosci.* 28, 421–426.
- Scoging, H., 1989. Runoff generation and sediment mobilisation by water. In: Thomas, D.S.G. (Ed.), *Arid Zone Geomorphology*. Belhaven Press, London, pp. 89–116. Book series, vol.
- Shaw, P.A., Thomas, D.S.G., 1989. Playas, pans and salt lakes. In: Thomas, D.S.G. (Ed.), *Arid Zone Geomorphology*. Belhaven Press, London, pp. 184–204. Book series, vol.
- Sun, X., Wang, P., 2005. How old is the Asian monsoon system? Palaeobotanical records from China. *Palaeogeogr. Palaeoclimatol. Palaeoecol.* 222, 181–222.
- Tan, H., Ma, H., Wei, H., Xu, J., Li, T., 2006. Chlorin, sulphur and oxygen isotopic constraints on ancient evaporite deposit in the Western Tarim Basin, China. *Geochem. J.* 40, 569–577.
- Tauxe, L., 1998. *Paleomagnetic Principles and Practice*. Kluwer Academic Publishers, Dordrecht, pp. 1–299.
- Villa, G., Fiorini, C., Pea, L., Bohaty, S., Persico, D., 2008. Middle Eocene–late Oligocene climate variability: calcareous nannofossil response at Kerguelen Plateau, Site 748. *Mar. Micropaleontol.* 69, 173–192.
- Vonhof, H.B., Smit, J., Brinkhuis, H., Montanari, A., Nederbragt, A.J., 2000. Global cooling accelerated by early late Eocene impacts? *Geology* 28, 687–690.
- Wang, C., Zhao, X., Liu, Z., Lippert, P.C., Graham, S.A., Coe, R.S., Yi, H., Zhu, L., Liu, S., Li, Y., 2008. Constraints on the early uplift history of the Tibetan Plateau. *Proc. Natl Acad. Sci.* 105, 4987–4992.
- Warren, J.K., 2006. *Evaporites: Sediments, Resources and Hydrocarbons*. Springer-Verlag, Berlin-Heidelberg, p. 1035.
- Westerhold, T., Röhl, U., 2009. High resolution cyclostratigraphy of the early Eocene – new insights into the origin of the Cenozoic cooling trend. *Climate Past* 5, 309–327.
- Wright, P.V., Marriott, S.B., 2007. The dangers of taking mud for granted: lessons from Lower Old Red Sandstone dryland river systems of South Wales. *Sed. Geol.* 195, 91–100.
- Xiao, G.Q., Abels, H.A., Yao, Z., Dupont-Nivet, G., Hilgen, F.J., 2010. Asian aridification linked to the first step of the Eocene–Oligocene climate Transition (EOT) in obliquity-dominated terrestrial records (Xining Basin, China). *Climate Past* 6, 501–513.
- Yeichieli, Y., Wood, W.W., 2002. Hydrogeologic processes in saline systems: playas, sabkhas, and saline lakes. *Earth Sci. Rev.* 58, 343–365.
- Zachos, J., Pagani, M., Sloan, L., Thomas, E., Billups, K., 2001. Trends, rhythms, and aberrations in global climate 65 Ma to present. *Science* 292, 686–693.
- Zhai, Y.P., Cai, T.L., 1984. The Tertiary system of Gansu province. *Gansu Geol.* 1–40 (in Chinese).
- Zhang, P.-Z., Molnar, P., Downs, W.R., 2001. Increased sedimentation rates and grain sizes 2–4 Myr ago due to the influence of climate change on erosion rates. *Nature* 410, 891–897.
- Zhang, Z.S., Wang, H.J., Guo, Z.T., Jiang, D.B., 2007. Impacts of tectonic changes on the reorganisation of the Cenozoic paleoclimatic patterns in China. *Earth Planet. Sci. Lett.* 257, 622–634.